

Article

Investigation of a Separated Short-Wavelength Peak in InGaN Red Light-Emitting Diodes

Pavel Kirilenko, Zhe Zhuang, Daisuke Iida, Martin Velazquez-Rizo and Kazuhiro Ohkawa *

Computer, Electrical and Mathematical Sciences and Engineering (CEMSE) Division, King Abdullah University of Science and Technology (KAUST), Thuwal 23955-6900, Saudi Arabia; pavel.kirilenko@kaust.edu.sa (P.K.); zhe.zhuang@kaust.edu.sa (Z.Z.); daisuke.iida@kaust.edu.sa (D.I.); martin.velazquezrizo@kaust.edu.sa (M.V.-R.)
* Correspondence: kazuhiro.ohkawa@kaust.edu.sa

Abstract: We fabricated indium gallium nitride (InGaN) red light-emitting diodes (LEDs) with a peak emission wavelength of 649 nm and investigated their electroluminescence (EL) properties. An additional separated peak in the EL spectrum of the red LEDs at 20 mA was observed at 465 nm. This additional peak also exhibits a blue-shift with increasing currents as does the main emission peak. Using high-resolution microscopy, we observed many point-like emission spots in the EL emission images at the currents below 1 mA. However, these emission spots cannot be identified at currents above 5 mA because the red emission from quantum wells (QWs) is much stronger than that emitted by these spots. Finally, we demonstrate that these emission spots are related to the defects generated in red QWs. The measured In content was lower at the vicinity of the defects, which was regarded as the reason for separated short-wavelength emission in red InGaN LEDs.

Keywords: InGaN; light-emitting diode; localized emission; electroluminescence mapping; multimicroscopy



Citation: Kirilenko, P.; Zhuang, Z.; Iida, D.; Velazquez-Rizo, M.; Ohkawa, K. Investigation of a Separated Short-Wavelength Peak in InGaN Red Light-Emitting Diodes. *Crystals* **2021**, *11*, 1123. <https://doi.org/10.3390/cryst11091123>

Academic Editors: Haiding Sun, Bharat Jalan, Shibing Long, Yuhao Zhang, Rajendra Singh, Xuelin Yang, Yuji Zhao, Bin Liu and Julien Brault

Received: 24 August 2021
Accepted: 9 September 2021
Published: 15 September 2021

Publisher's Note: MDPI stays neutral with regard to jurisdictional claims in published maps and institutional affiliations.



Copyright: © 2021 by the authors. Licensee MDPI, Basel, Switzerland. This article is an open access article distributed under the terms and conditions of the Creative Commons Attribution (CC BY) license (<https://creativecommons.org/licenses/by/4.0/>).

1. Introduction

III-nitride semiconductors have become popular materials for constructing light-emitting diodes (LEDs) as a result of several breakthroughs in the epitaxial growth, doping techniques, and device performances of these semiconductors [1–4]. With different in fractions in the InGaN alloy, the material band gap can be tuned from 0.67 to 3.42 eV [5,6]. Low in content in InGaN blue LEDs present external quantum efficiencies up to 84% [7] whereas LEDs with high in content have much lower efficiencies [8–10]. The main factors corresponding to the low efficiency for high-In-content LEDs are low-temperature growth [11,12] and large lattice mismatch (11%) between InN and GaN. Introduction of high growth temperature and strain relaxation techniques helped to significantly improve the efficiency of the long-wavelength emitting InGaN LEDs [13,14].

However, the long-wavelength emitting InGaN LEDs show additional emission peaks in the blue-green range in their electroluminescence (EL) spectra [8,15–18]. This phenomenon hinders the realization of pure-red InGaN LEDs. This obstacle can be critical for the fabrication of monolithically integrated micro-LED displays because pure red is impossible to realize with this additional blue component. The presence of the additional emission in high-In-content InGaN LEDs is generally attributed to the poor miscibility between InN and GaN [19]. Additionally, in phase separation tends to appear because of the strain caused by lattice mismatch in the active region [20]. All of these phenomena would lead to the in concentration fluctuation in the high-In-content InGaN QWs and possibly result in the additional emission. However, minimal evidence that directly explains the origin of the additional component in the EL spectra exists.

In this study, we observed the additional emission component from the EL spectrum of our red InGaN LEDs. The emission behaviors of the additional component were first investigated using EL measurements at different currents at room temperature (RT). The

EL mappings under high-resolution microscopy were used to examine the luminescence patterns at different currents. By precisely marking the positions of the localized emission spots, we finally measured the structures and elements of the localized emission spots and provided direct evidence for the origin of the additional short-wavelength emission.

2. Materials and Methods

The LED structure was grown on the *c*-plane patterned sapphire substrate using metalorganic vapor-phase epitaxy (MOVPE) in a single-wafer horizontal reactor. The precursors for Ga, Al, In, and N were trimethylgallium (TMGa), trimethylaluminum (TMAI), trimethylindium (TMIn), and ammonia (NH₃), respectively. The cross-sectional schematic of the red LED structure is shown in Figure 1. The n-side and active regions consisted of an n-GaN:Si 6 μm layer, an n-Al_{0.03}Ga_{0.97}N:Si (1 μm) layer, 15 superlattices (SLs) of GaN (6 nm)/In_{0.08}Ga_{0.92}N (2 nm), an n-GaN:Si (15 nm), an In_{0.2}Ga_{0.8}N (2 nm) blue single QW with GaN (2 nm)/Al_{0.13}Ga_{0.87}N (18 nm)/GaN (3 nm) barrier layers, and InGaN (2.5 nm) red double QWs as an active region with AlN interlayer (1.2 nm)/GaN (2 nm)/Al_{0.13}Ga_{0.87}N (18 nm)/GaN (3 nm) barrier layers. GaN substituted the Al_{0.13}Ga_{0.87}N part in the upper barrier of the second red QW. An additional GaN layer (15 nm) was grown in the active region. In this hybrid QW design, the bottom blue QW produced no emission but caused a significant increase in red emission from the top red DQW. The AlN interlayers suppressed the decomposition of the high-In-content InGaN QWs during barrier layer growth at higher temperatures. The AlGaN barrier layer also provided strain compensation to improve the crystalline quality of InGaN QWs. Finally, a p-GaN:Mg layer (100 nm) and a p⁺-GaN:Mg contact layer (10 nm) were grown. The LEDs were fabricated according to the standard methods [21]. A 90 nm-thick indium tin oxide (ITO) layer was utilized as a transparent conductive layer. Mesa-etching was carried out via inductively-coupled plasma etching to expose the n-Al_{0.03}Ga_{0.97}N layer. The n- and p-electrodes consisted of Cr (50 nm)/Ni (20 nm)/Au (200 nm) using e-beam evaporation. The LED chip size was 250 × 650 μm².

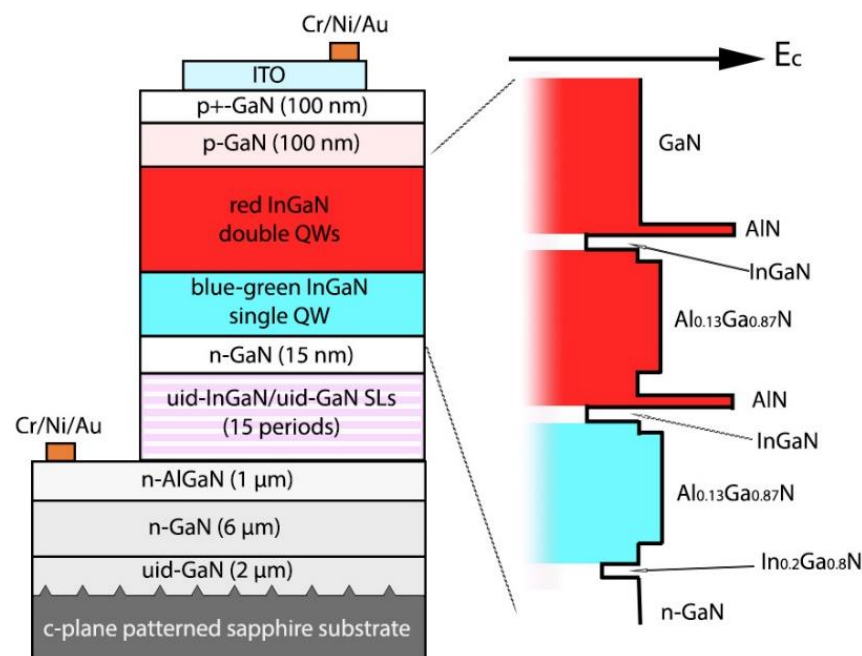


Figure 1. Red indium gallium nitride (InGaN) light-emitting diode (LED) epistructure and conduction band profile in the active region.

The EL spectra were recorded after electrical pumping of the LEDs at the probe station. The EL mapping was performed using the optical with built-in 5× zoom and 100× optics, whose spatial resolution is 0.6 μm. The devices were under DC current injection at RT. We

found some landmarks for the localized emission area from the EL mappings. After that, the ITO layer was removed by the hydrochloric acid (HCl) wet etching to expose p-GaN. The surface morphology was re-examined using the scanning electron microscope (SEM). We then compared the EL mapping and the SEM image using some landmarks, such as large defect clusters. Based on this comparison, we could find the exact position of the point-like emission sources corresponding to the additional short-wavelength emission. We then fabricated the lamella using focused ion beam (FIB) methods. Finally, we measured the structures and elemental mapping of the lamella by scanning transmission electron microscope (STEM) installed with electron dispersive X-ray spectroscopy (EDS).

3. Results and Discussion

Figure 2 shows the typical EL spectrum of our red LED at 20 mA. A main red peak at a wavelength of 649 nm was observed, but a blue peak at a wavelength of 465 nm also had appeared. The main red peak exhibited a full-width at half maximum (FWHM) of 62 nm, which was much larger compared to InGaN green and blue LEDs. The broad FWHM was caused by in fluctuations in high-In-content InGaN QWs [8]. In case of the additional blue peak, we did not attribute it to the blue QW in our epitaxial structure because the intensity of the additional peak was only a small percentage of the main peak. If the emission originated from the blue QW, the intensity should be even stronger than the main peak due to higher efficiency of the blue QW [22].

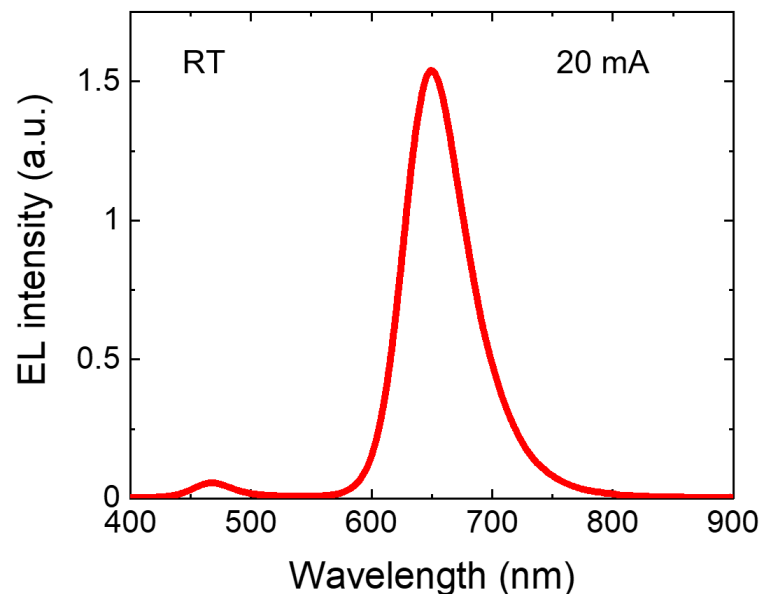


Figure 2. Electroluminescence (EL) spectrum of the red LED at 20 mA.

Before clarifying the origin of the additional peak, we first investigated the EL performance of this additional peak at currents ranging from 1 to 50 mA. The current dependence of the peak positions is shown in Figure 3a. Both the main and additional peaks exhibited an obvious blue-shifts of 55 and 19 nm at currents of 1 to 50 mA, respectively. This peak wavelength blue-shift for *c*-plane InGaN LEDs is a common feature, which is mostly due to the strong quantum confined Stark effect (QCSE) and band-filling effect [8]. However, the blue QWs usually would undergo a lower peak wavelength blue-shift (<10 nm) due to a smaller QCSE in low-In-content QWs [23]. Therefore, this large blue-shift of the additional peak in our red LEDs should be mainly attributed to the band-filling effect. It means that the additional peak did not originate from the blue QW, but rather from the localized states.

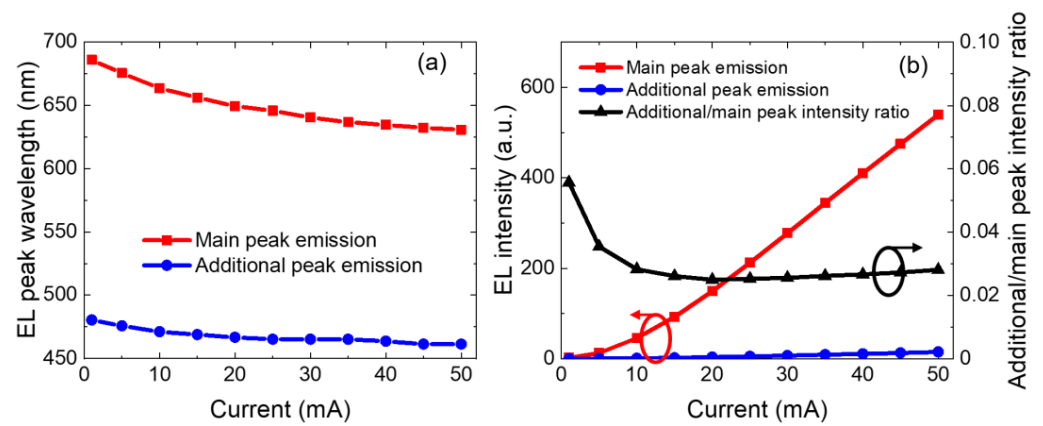


Figure 3. Current dependence of (a) the peak wavelengths, and (b) EL intensity and intensity ratio for additional short-wavelength and red quantum well (QW) emission.

Figure 3b shows the EL intensities of the main and additional peaks and their intensity ratios (additional peak/main peak) at different currents. The EL intensities of the main and additional peaks increased with increases in the currents, but the increment behavior is different. At currents above 10 mA, the main and additional peak intensities increased almost linearly with the current. Therefore, their intensity ratio almost remained constant, which illustrated that the current injection condition was the same for the two peaks. However, at currents below 10 mA, the intensity ratio was larger, as shown in Figure 3b. Therefore, a larger ratio indicated that the current injection might be different for the main and additional peaks at low currents.

To confirm this assumption, we examined the EL mappings at low currents ranging from 0.5 to 5 mA, as shown in Figure 4. The n-pad was selected as a landmark to guarantee the same EL mapping area. Exposure time for the camera was adjusted to avoid overexposures at different currents. At 0.5 mA (Figure 4a), we could observe many separated point-like emission sources instead of red QWs. The separated emission corresponded to different emission wavelengths ranging from blue, green, and yellow to red. We believed that these separated emission spots might be the origin of the additional peak in the EL spectrum.

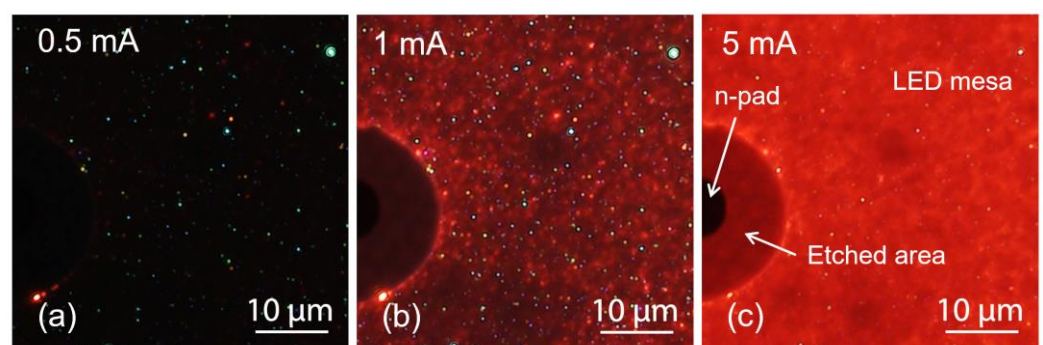


Figure 4. EL mappings at the current of (a) 0.5 mA, (b) 1 mA and (c) 5 mA.

When the current increased to 1 mA in Figure 4b, the red QWs started to emit but the emissions were not very uniform. After increasing the current to 5 mA, homogeneous emission from red QWs could be observed in Figure 4c. This homogeneous emission was from the InGaN red QWs and corresponded to the main peak in the EL spectrum. In this case, some separated emission spots were difficult to distinguish. The localized emission spot density could be estimated as $4.4 \pm 0.25 \times 10^7 \text{ cm}^{-2}$ on average. Additionally, the separated emission with blue color in Figure 4a,b seemed to be dominant, which could explain the additional blue peak in the EL spectrum.

We investigated the structure of these localized emission areas further to explain why the current passed more easily through these areas. Some recognizable surface defects in the EL mappings were selected as landmarks. Based on these landmarks, we could precisely find the localized emission area based on SEM and used FIB to fabricate the lamella that contained the localized emission spots for STEM measurements, which were marked as white lines in Figure 5a,b.

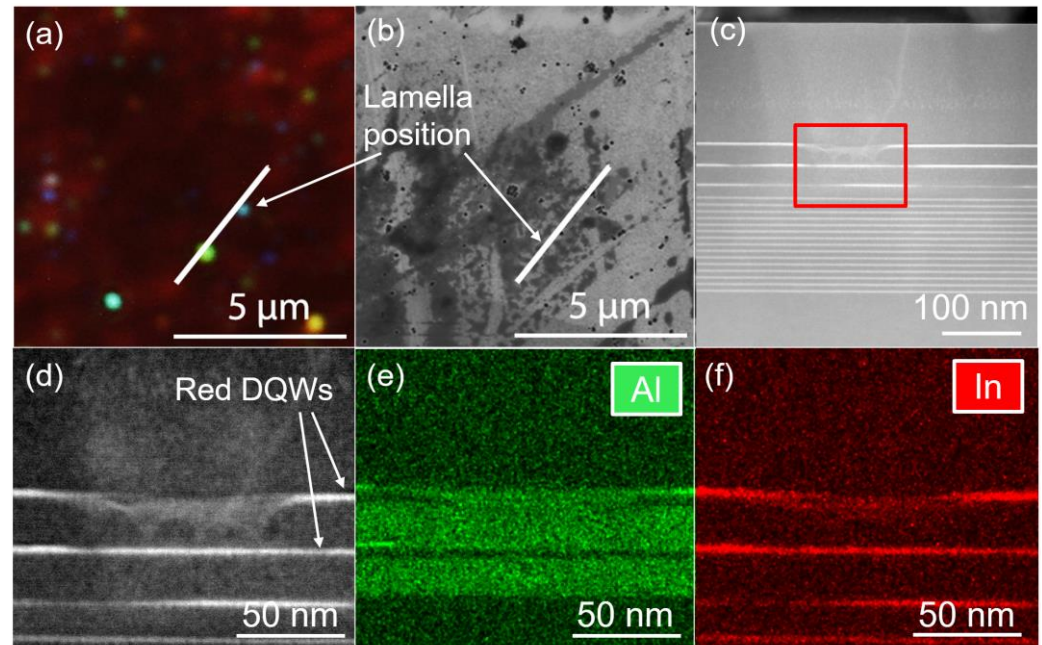


Figure 5. (a) EL mapping and (b) scanning electron microscope (SEM) image used for the lamella positioning. (c) Scanning transmission electron microscope (STEM) image and (d) high-resolution STEM image of our active region structure. (e) Al and (f) In atom distribution mapping in the active region by STEM energy dispersive X-ray spectroscopy (EDS) measurements.

Figure 5c shows the cross-sectional STEM image of the selected separated emission spot in the lamella. An obvious defect was observed in this region, demonstrating that the separated emission was related to the defects generated in red QWs. This finding is reasonable for the easier current injection because the defects generally serve as leakage channels. Therefore, these separated emission spots would be first observed at low currents. The mechanism of the carrier leakage via tunneling, assisted by the defect levels, was previously reported [24,25]. However, those works contribute the point-like emission under low forward bias to the carrier leakage, from the quantum well layer to the defect levels in the electron blocking layer and p-GaN. This concept does not apply to the case of the additional emission having shorter wavelength than the quantum well, as we have observed.

The high-resolution STEM image for the defect area corresponding to the separated emission is shown in Figure 5d. The top red QW is not continuous and uniform in this figure. Therefore, the quality of the red QW in this region was not good. We also analyzed the elements for this defect area using STEM EDS elemental mapping. Figure 5e shows the Al element was distributed in the QW capping layer and barriers, which agreed well with our growth design. However, the Al atoms diffused into the red QW in the defect region. The In distribution was also not uniform in the top red QW, as shown in Figure 5f. The lower level of brightness in Figure 5f indicates that the In content in this region was lower compared to other areas of higher brightness. As a result, this region corresponded to the separated emission and exhibited a shorter wavelength emission than the red QWs, a finding that was consistent with the EL spectrum and mappings. We presumed that

the lower in content originated from the decomposition of the InGaN red QW, while the capping and barrier layers were growing.

4. Conclusions

In this study, we fabricated 649 nm InGaN red LEDs and investigated the properties of the additional peak in the EL spectrum. This additional peak exhibited a 19 nm blue-shift after increasing the current from 1 to 50 mA. Based on the EL mappings, we attributed that the additional peak came from many separated point-like emission spots in our red LEDs. By precisely analyzing the structure and elements of the separated emission spots, we demonstrated that the separated emission spots were related to the defect areas that contained lower in contents in red QWs. These results were helpful for understanding the EL performance of the red InGaN QWs and may be useful as guidelines to improve the quality of high-In-content QWs in the future.

Author Contributions: Conceptualization, P.K. and K.O.; methodology, P.K., Z.Z., M.V.-R. and D.I.; software, P.K.; validation, Z.Z., D.I. and M.V.-R.; formal analysis, Z.Z. and D.I.; investigation, P.K.; resources, P.K., Z.Z., M.V.-R. and D.I.; data curation, P.K., Z.Z. and D.I.; writing—original draft preparation, P.K.; writing—review and editing, Z.Z.; visualization, P.K.; supervision, K.O.; project administration, D.I.; funding acquisition, K.O. All authors have read and agreed to the published version of the manuscript.

Funding: King Abdullah University of Science and Technology (BAS/1/1676-01-01).

Data Availability Statement: Data underlying the results presented in this paper are not publicly available at this time but may be obtained from the authors upon reasonable request.

Acknowledgments: The fabrication processes in this work were supported by Nanofabrication Core Lab.

Conflicts of Interest: The authors declare no conflict of interest.

References

1. Amano, H.; Sawaki, N.; Akasaki, I.; Toyoda, Y. Metalorganic vapor phase epitaxial growth of a high quality GaN film using an AlN buffer layer. *Appl. Phys. Lett.* **1986**, *48*, 353–355. [[CrossRef](#)]
2. Nakamura, S. GaN Growth Using GaN Buffer Layer. *Jpn. J. Appl. Phys.* **1991**, *30*, L1705–L1707. [[CrossRef](#)]
3. Nakamura, S.; Iwasa, N.; Senoh, M.; Mukai, T. Hole Compensation Mechanism of P-Type GaN Films. *Jpn. J. Appl. Phys.* **1992**, *31*, 1258–1266. [[CrossRef](#)]
4. Nakamura, S.; Mukai, T.; Senoh, M. Candela-class high-brightness InGaN/AlGaIn double-heterostructure blue-light-emitting diodes. *Appl. Phys. Lett.* **1994**, *64*, 1687–1689. [[CrossRef](#)]
5. Brunner, D.; Angerer, H.; Bustarret, E.; Freudenberg, F.; Höppler, R.; Dimitrov, R.; Ambacher, O.; Stutzmann, M. Optical constants of epitaxial AlGaIn films and their temperature dependence. *J. Appl. Phys.* **1997**, *82*, 5090–5096. [[CrossRef](#)]
6. Araki, T.; Saito, Y.; Yamaguchi, T.; Kurouchi, M.; Nanishi, Y.; Naoi, H. Radio frequency-molecular beam epitaxial growth of InN epitaxial films on (0001) sapphire and their properties. *J. Vac. Sci. Technol. B Microelectron. Nanometer Struct. Process. Meas. Phenom.* **2004**, *22*, 2139–2143. [[CrossRef](#)]
7. Narukawa, Y.; Ichikawa, M.; Sanga, D.; Sano, M.; Mukai, T. White light emitting diodes with super-high luminous efficacy. *J. Phys. D Appl. Phys.* **2010**, *43*, 354002. [[CrossRef](#)]
8. Mukai, T.; Yamada, M.; Nakamura, S. Characteristics of InGaN-Based UV/Blue/Green/Amber/Red Light-Emitting Diodes. *Jpn. J. Appl. Phys.* **1999**, *38*, 3976–3981. [[CrossRef](#)]
9. Mukai, T. Recent progress in group-III nitride light-emitting diodes. *IEEE J. Sel. Top. Quantum Electron.* **2002**, *8*, 264–270. [[CrossRef](#)]
10. Krames, M.R.; Shchekin, O.B.; Mueller-Mach, R.; Mueller, G.O.; Zhou, L.; Harbers, G.; Craford, M.G. Status and Future of High-Power Light-Emitting Diodes for Solid-State Lighting. *J. Disp. Technol.* **2007**, *3*, 160–175. [[CrossRef](#)]
11. Nagatomo, T.; Kuboyama, T.; Minamino, H.; Omoto, O. Properties of Ga_{1-x}In_xN Films Prepared by MOVPE. *Jpn. J. Appl. Phys.* **1989**, *28*, L1334–L1336. [[CrossRef](#)]
12. Yoshimoto, N.; Matsuoka, T.; Sasaki, T.; Katsui, A. Photoluminescence of InGaIn films grown at high temperature by metalorganic vapor phase epitaxy. *Appl. Phys. Lett.* **1991**, *59*, 2251–2253. [[CrossRef](#)]
13. Ohkawa, K.; Watanabe, T.; Sakamoto, M.; Hirako, A.; Deura, M. 740-nm emission from InGaIn-based LEDs on c-plane sapphire substrates by MOVPE. *J. Cryst. Growth* **2012**, *343*, 13–16. [[CrossRef](#)]
14. Hashimoto, R.; Hwang, J.; Saito, S.; Nunoue, S. High-efficiency green-yellow light-emitting diodes grown on sapphire (0001) substrates. *Phys. Status Solidi C* **2013**, *10*, 1529–1532. [[CrossRef](#)]

15. Hwang, J.I.; Hashimoto, R.; Saito, S.; Nunoue, S. Development of InGaN-based red LED grown on (0001) polar surface. *Appl. Phys. Express* **2014**, *7*, 071003. [[CrossRef](#)]
16. Alhassan, A.I.; Farrell, R.M.; Saifaddin, B.; Mughal, A.; Wu, F.; DenBaars, S.P.; Nakamura, S.; Speck, J.S. High luminous efficacy green light-emitting diodes with AlGaIn cap layer. *Opt. Express* **2016**, *24*, 17868–17873. [[CrossRef](#)]
17. Iida, D.; Zhuang, Z.; Kirilenko, P.; Velazquez-Rizo, M.; Najmi, M.A.; Ohkawa, K. 633-nm InGaIn-based red LEDs grown on thick underlying GaN layers with reduced in-plane residual stress. *Appl. Phys. Lett.* **2020**, *116*, 162101. [[CrossRef](#)]
18. Zhuang, Z.; Iida, D.; Ohkawa, K. Effects of size on the electrical and optical properties of InGaIn-based red light-emitting diodes. *Appl. Phys. Lett.* **2020**, *116*, 173501. [[CrossRef](#)]
19. Kim, K.S.; Son, J.K.; Lee, S.N.; Sung, Y.J.; Paek, H.S.; Kim, H.K.; Kim, M.Y.; Ha, K.H.; Ryu, H.Y.; Nam, O.H.; et al. Characteristics of long wavelength InGaIn quantum well laser diodes. *Appl. Phys. Lett.* **2008**, *92*, 101103. [[CrossRef](#)]
20. El-Masry, N.A.; Piner, E.L.; Liu, S.X.; Bedair, S.M. Phase separation in InGaIn grown by metalorganic chemical vapor deposition. *Appl. Phys. Lett.* **1998**, *72*, 40–42. [[CrossRef](#)]
21. Zhuang, Z.; Iida, D.; Kirilenko, P.; Velazquez-Rizo, M.; Ohkawa, K. Optimal ITO transparent conductive layers for InGaIn-based amber/red light-emitting diodes. *Opt. Express* **2020**, *28*, 12311–12321. [[CrossRef](#)] [[PubMed](#)]
22. Iida, D.; Zhuang, Z.; Kirilenko, P.; Velazquez-Rizo, M.; Ohkawa, K. High-color-rendering-index phosphor-free InGaIn-based white light-emitting diodes by carrier injection enhancement via V-pits. *Appl. Phys. Lett.* **2020**, *117*, 172103. [[CrossRef](#)]
23. Lu, C.; Wang, L.; Lu, J.; Li, R.; Liu, L.; Li, D.; Liu, N.; Li, L.; Cao, W.; Yang, W.; et al. Investigation of the electroluminescence spectrum shift of InGaIn/GaN multiple quantum well light-emitting diodes under direct and pulsed currents. *J. Appl. Phys.* **2013**, *113*, 13102. [[CrossRef](#)]
24. Han, D.P.; Oh, C.H.; Kim, H.; Shim, J.I.; Kim, K.S.; Shin, D.S. Conduction mechanisms of leakage currents in InGaIn/GaN-based light-emitting diodes. *IEEE Trans. Electron Devices* **2015**, *62*. [[CrossRef](#)]
25. Meneghini, M.; Vaccari, S.; Trivellin, N.; Zhu, D.; Humphreys, C.; Butendheich, R.; Leirer, C.; Hahn, B.; Meneghesso, G.; Zanoni, E. Analysis of Defect-related localized emission processes in InGaIn/GaN-based LEDs. *IEEE Trans. Electron Devices* **2012**, *59*. [[CrossRef](#)]